11-1-2021

Ultrasound regulated flexible protein materials: Fabrication, structure and physical-biological properties.

Bowen Cai

Hanling Gu

Fang Wang

Kyle Printon

Zhenggui Gu

See next page for additional authors

Recommended Citation

Bowen, Cai; Gu, Hangling; Wang, Fang; Printon, Kyle; Gu, Zhenggui; & Hu; Xiao. Ultrasound regulated flexible protein materials: Fabrication, structure and physical-biological properties. Ultrasonics Sonochemistry, November 2021, Volume 79, 105800.

Ultrasonics Sonochemistry 79 (2021) 105800

Contents lists available at ScienceDirect

Ultrasonics Sonochemistry

journal homepage: www.elsevier.com/locate/ultson

Ultrasound regulated flexible protein materials: Fabrication, structure and physical-biological properties

Bowen Cai [a,b], Hanling Gu [a,b], Fang Wang [a,b,*], Kyle Printon [c,d], Zhenggui Gu [b], Xiao Hu [c,d,e,*]

[a] Center of Analysis and Testing, Nanjing Normal University, Nanjing 210023, China
[b] School of Chemistry and Materials Science, Nanjing Normal University, Nanjing 210023, China
[c] Department of Physics and Astronomy, Rowan University, Glassboro, NJ 08028, USA
[d] Department of Biomedical Engineering, Rowan University, Glassboro, NJ 08028, USA
[e] Department of Molecular and Cellular Biosciences, Rowan University, Glassboro, NJ 08028, USA

ARTICLE INFO

Keywords:
Ultrasonic treatment
Beta sheet
Silk
Insolubility
Structural transformation
Biological property

ABSTRACT

Ultrasound can be used in the biomaterial field due to its high efficiency, easy operation, no chemical treatment, repeatability and high level of control. In this work, we demonstrated that ultrasound is able to quickly regulate protein structure at the solution assembly stage to obtain the designed properties of protein-based materials. Silk fibroin proteins dissolved in a formic acid-$CaCl_2$ solution system were treated in an ultrasound with varying times and powers. By altering these variables, the silks physical properties and structures can be fine-tuned and the results were investigated with Fourier transform infrared spectroscopy (FTIR), X-ray diffraction (XRD), scanning electron microscopy (SEM), differential scanning calorimetry (DSC), thermogravimetric analysis (TGA), dynamic mechanical analysis (DMA), gas permeability and water contact angle measurements. Ultrasonic treatment aids the interactions between the calcium ions and silk molecular chains which leads to increased amounts of intermolecular β-sheets and α-helix. This unique structural change caused the silk film to be highly insoluble in water while also inducing a hydrophilic swelling property. The ultrasound-regulated silk materials also showed higher thermal stability, better biocompatibility and breathability, and favorable mechanical strength and flexibility. It was also possible to tune the enzymatic degradation rate and biological response (cell growth and proliferation) of protein materials by changing ultrasound parameters. This study provides a unique physical and non-contact material processing method for the wide applications of protein-based biomaterials.

1. Introduction

Natural silk, which is highly available due to its use in the textile industry, has become a widely studied protein material in the biomedical and bioengineering field. As a renewable resource available in large quantities, silk is also nontoxic and highly biocompatible [1–6]. Natural silk fibers are comprised of silk fibroin protein fibers with a glycoprotein coating. Silk fibroin (SF) is a complex molecular chain built from amino acids that form a large segment (H-chain), a small segment (L-chain) and a small glycoprotein (P25 protein). Among them, the relatively hydrophobic H-chain fibroin is linked to the hydrophilic and relatively elastic L-chain fibroin [1,7–8]. Silk fibroin chains initially exist as aggregates and micelles in liquid silk within the silkworm glands, which plays an important role in the formation of β-sheet structure. These β-sheet structures generally lead to a crystallinity of about 60 ~ 75% in the silk proteins [1,7–10]. However, it is extremely difficult to reach these levels of crystallinity in regenerated silk fibroins. The percentage of β-sheet structures in the regenerated silk material directly influences silks degradability, thermal stability and mechanical properties. Therefore, methods to prepare and dissolve silk fibroins that could allow for structural regeneration of the initial silk secondary structures were intensively investigated [11–15]. Numerous studies have used various solvents that imitate silkworm spinnerets to influence the conformation and properties of regenerated silk fibroin macromolecules [11–16]. It has also been suggested that the conformation of silk fibroin is related to the solvents during the regeneration process. Organic polar solvents can lead to the formation of β-sheet structures, while non-polar solvents have been shown to interact with silk fibroin causing the formation of

* Corresponding authors at: Center of Analysis and Testing, Nanjing Normal University, Nanjing 210023, China (F. Wang). Department of Physics and Astronomy, Rowan University, Glassboro, NJ 08028, USA (X. Hu).
E-mail addresses: wangfang@njnu.edu.cn (F. Wang), hu@rowan.edu (X. Hu).

https://doi.org/10.1016/j.ultsonch.2021.105800
Received 3 August 2021; Received in revised form 14 October 2021; Accepted 15 October 2021
Available online 16 October 2021

random coils and α-helix structures [9,11–16].

Ultrasound can produce a series of compressional waves which are interspaced by medium propagation to construct divergent, planar or focused sound fields through the transmission of mechanical vibrational energy [17–20]. Ultrasound has been found to produce mechanical, acoustic-thermal, chemical and biological effects by directly altering the physical and chemical properties of a material [21–28]. Ultrasound was previously often used to prepare biologically functional hydrogels with specific mechanical properties [19], drug delivery carriers for targeted therapy [20] and environmentally friendly adsorption and filtration materials [21]. Susanin *et al.* [22] found that the proportion of α-helix conformation decreased and β-turns and β-sheets structure increased after 24 kHz ultrasound treatment with a duration of 5 min for silk fibroin proteins regenerated from a LiBr-based aqueous system. Li *et al.* [23] revealed that the initial random coils and β-turns of myofibrillar proteins could be transformed into an α-helix or β-sheet structure in response to an ultrasound-microwave treatment. Su and Cavaco-Paulo [24] reviewed the effects of ultrasound on protein functionality and revealed that ultrasound is an effective tool for the formation and stabilization of protein emulsions and dispersions, which provides energy for conformational changes in protein structure, and acts as a medium for the intensification of enzymatic process. Sliva *et al.* [25] investigated the mechanism of microsphere formation from bovine serum albumin and silk fibroin using ultrasound. It was found that when the high shear forces generated from ultrasound were applied to the aqueous/organic solvent system, the accommodation of SF to the biphasic system interface tended to promote self-assembly of the β-sheet structure, while the globular proteins retained their secondary structures during the particle formation. Although ultrasound has been shown to be an effective method for altering the structure of proteins, its ability to induce conformational transformations of polypeptides and its transmission mechanism are still unclear.

In this work, the structural transformation and physical-biological property changes of silk fibroin (SF) films fabricated in a formic acid-$CaCl_2$ system was comparatively demonstrated under different ultrasonic time and power. The regenerated silks morphology, secondary structures such as intermolecular and intramolecular β-sheet were investigated by SEM and FTIR. The silks crystallinity and thermodynamic parameters were also characterized by XRD and DSC, respectively. Furthermore, their thermal stability, mechanical properties, air permeability, as well as the hydrophilicity were investigated. Finally, a detailed mechanism of ultrasound on silk fibroin materials was proposed in this study.

2. Experimental section

2.1. Materials preparation

Bombyx Mori silkworm cocoons from China were first degummed into silk fibroin fibers, and dissolved into a formic acid-$CaCl_2$ solution (4.00 wt%) to form the 8.00 wt% silk fibroin solution [4]. An ultrasonic equipment (Ymnl-950Y, Nanjing Emmanuel Instrument & Equipment Co., Ltd, China), composed of a probe-type ultrasound source equipped with a 2 mm diameter titanium microtip, is used for ultrasonic treatment of the silk fibroin solution. The output power of the machine can be controlled between 9 W and 950 W according to the amplitude ratio. The reaction vessel is an open glass cup with a diameter of 60 mm and a height of 72 mm. An equal volume of regenerated silk fibroin solution (about 50 mm high) was put into the reaction vessel each time, where the end of the probe source was 10 mm below the solution surface. The first group received ultrasonic treatment with 600 W power with time points of 0 min, 1 min, 5 min, 15 min and 30 min. The treated solution was then cast into films and washed with DI water for 5 mins to remove solvent residues. Finally, the silk films were vacuum dried for 48 hrs to form the final materials (Fig. 1). Samples of the first group are denoted as MSF, MSFT-1, MSFT-5, MSFT-15, MSFT-30 based on their treatment time. The second group received ultrasonic treatments with varying power of 100 W, 300 W, 500 W, 700 W and 800 W while the time stayed constant at 30 min.Te solution from the second group was prepared into films with the same method that was discussed in the first group (Fig. 1a). The samples in the second group were named as MSFP-100, MSFP-300, MSFP-500, MSFP-700, MSFP-800 based on their treatment powers.

The power intensity generated by the ultrasonic source is given by eqaution (1) [29]:

$$I = P_a^2(2\rho \hat{A}\cdot C)^{-1} \tag{1}$$

where I is the sound intensity, ρ and c are the medium density and the sound velocity, respectively, and P_a is the sound pressure amplitude, which is related to the time t and the frequency f of the wave. Ultrasound can generate bubbles which can diffuse in the fluid. Generally, the acoustic energy is transmitted to bubbles, which expand during the negative acoustic pressure, while contract during the positive one, and accumulate continuously to grow through a liquid medium. When the bubble resonance is reached, the sound pressure exceeds the threshold and the bubble collapse occurs, which releases huge energy and forms the phenomenon of ultrasonic cavitation. The velocity of the bubble is inversely proportional to the area of the circle from the center of the ultrasound, as described in eqaution (2) [30–31]:

$$\frac{u}{U} = \frac{R^2}{r^2} \tag{2}$$

$$K = \frac{1}{2}\rho \int_R^\infty u^2 \hat{A}\cdot 4\pi r^2 dr = 2\pi\rho U^2 R^3 \tag{3}$$

where R represents the radius of the bubble, U is the surface velocity at time t, u is the velocity at any distance r (>R) from the center of the bubble. The kinetic energy K of the bubble is given by eqaution (3) [30–31], where ρ is the density of the medium. When a bubble spreads from a collapsed to the surrounding fluid, the energy produced can accelerate the mass transfer rate between the interface, and the vapor liquid pressure also increases as the reaction temperature, which can accelerated the efficiency of the heterogeneous reaction. Therefore, the sound pressure, the hydrostatic pressure, the frequency, and the maximum density of the liquid can determine the bubble size of the cavitation, as shown in equation (4) and (5) [30]:

$$R_r = \sqrt{\frac{3\gamma P_\infty}{\rho\omega^2}} \tag{4}$$

$$R_{max} = \frac{4}{3\omega_a}(P_a - P_h)\left(\frac{2}{\rho P_a}\right)^{1/2}\left[1 + \frac{2}{3P_h}(P_a - P_h)\right]^{1/3} \tag{5}$$

where R_r and R_{max} are the bubble size and the maximum size of the bubble, respectively. γ is the specific heat ratio of the gas inside the bubble, P_∞ and P_h are the ambient fluid pressure and extra (hydrostatic) pressure, respectively. ρ is the liquid density, ω is the angular frequency of the ultrasound. The above equations can be predicted by an optimum power density during sonication, to obtain the maximum reaction rate.

2.2. Characterization

2.2.1. Scanning electron microscope

Scanning electron microscope (SEM, JSM-7600F, JEOL, Japan) was used to observe the morphology of different regenerated silk fibroin films. After being coated with conductive carbon double-layer tape, the sample was gold-plated (20 mA, 3 times, 30 s each time) by using a sputter coater (JFC-1600, JEOL, Japan) under voltage 5 ~ 10 kV and 15 mm distance.

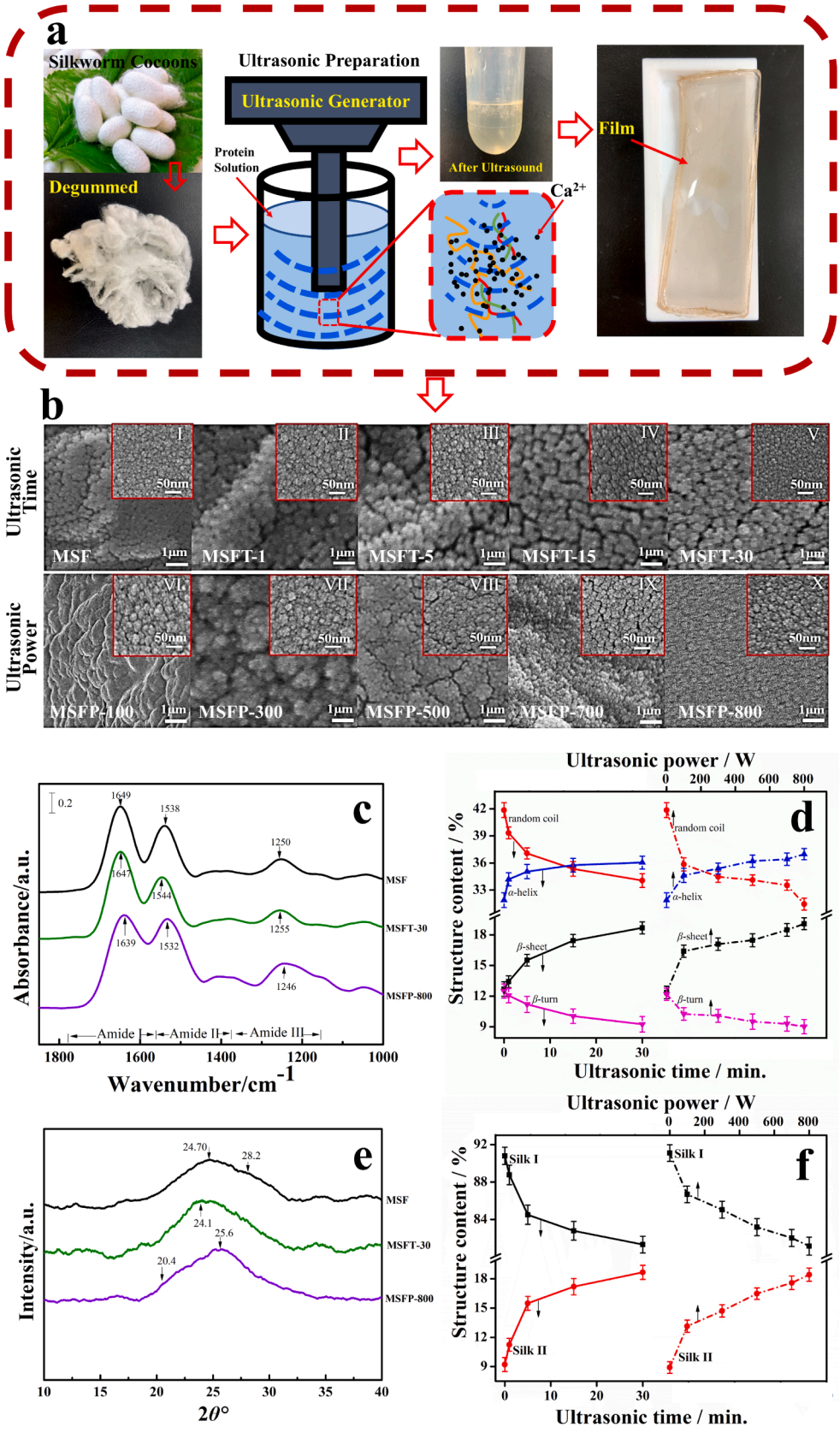

Fig. 1. (a) Schematic preparation of flexible silk fibroin (SF) protein materials using ultrasound. (b) SEM images of ultrasound-treated SF films for (MSF) 0, (MSFT-1) 1, (MSFT-5) 5, (MSFT-15) 15 and (MSFT-30) 30 min under 600 W power, and at (MSFP-100) 100 W, (MSFP-300) 300 W, (MSFP-500) 500 W, (MSFP-700) 700 W and (MSFP-800) 800 W intensity for 30 min, respectively (1 μm scale bar), where the inserted (I-X) images correspond to their local enlarged views (50 nm scale bar). (c) FTIR absorbance spectra of films MSF 0, MSFT-30 and MSFP-800 in the 1000 ~ 1820 cm^{-1} region. (d) The protein secondary structure contents in ultrasound-treated SF films calculated by a curve fitting method for Amide I region. (e) XRD spectra of films MSF 0, MSFT-30 and MSFP-800. (f) The Silk I and II contents in ultrasound-treated SF films, calculated from XRD curves.

2.2.2. Fourier-Transform infrared spectroscopy

Fourier transform infrared spectrometer (FTIR, Nicolet-Nexus 670, Nicolet, USA) was used to obtain the infrared spectrogram of these silk fibroin films. The spectrum was recorded in the wavenumber range of 400 ~ 4000 cm^{-1} at 4 cm^{-1} and 128 times each scan. The curve-fit of peaks in the amide I region was performed using the Origin software.

2.2.3. X-ray diffraction

X-ray diffractometer (XRD, D/max 2500/PC, Rigaku, Japan) was used to measure the crystal structure of sample with the tube pressure of 40 kV, the tube flow of 100 mA, the diffraction angle 2θ range of 5° ~ 50°, and the scanning speed of 5°·min^{-1}.

2.2.4. Differential scanning calorimetry

Thermal properties of samples were obtained using thermal analysis (STA7300 TG-DTA, Hitachi, Japan) in nitrogen atmosphere with a flow rate of 50 mL·min^{-1} during ambient temperature to 650 °C at a heating rate of 10 °C·min^{-1}. In order to understand the glass transition process of different silk fibroin samples, step-scan modulation differential scanning calorimeter (SSDSC, Diamond DSC, PerkinElmer, USA) was used with a heating rate of 10℃ min^{-1}, a 2 ℃ step and an isothermal time of 1 min.

2.2.5. Thermogravimetric analysis

Thermogravimetric analysis (TG, Pyris 1, PerkinElmer, USA) was used to measure the mass percentage changes with temperature for different silk fibroin samples. Sample with a mass of about 5–6 mg was taken into pan, heated from ambience temperature to 650 °C at a heating rate of 10 °C·min^{-1} in a nitrogen atmosphere with a gas flow of 50 mL min^{-1}. The first derivative of the thermogravimetric analysis curve (DTG) was also presented to reflect the degradation rate and the intermediate degradation temperatures.

2.2.6. Water contact angle measurement

The surface wettability of silk films under different ultrasonic conditions was measured and analyzed by a water contact angle meter (WCA, DSA30S, KRUSS, Germany) through dropping 2 μl of pure water droplets on the random surface of the sample for 10 s.

2.2.7. Bio-enzymatic degradation

Protease XIV was dissolved in a PBS (pH = 7.2) buffer solution with a concentration of 0.2 mg/ml (1.4U/ml). The silk fibroin film with a mass of 40 ± 5 mg was then placed into a centrifuge tube with 5 mL of protease solution and was place in a constant 37 °C water bath. After incubating for 6, 24, 72 h respectively, the samples were vacuum-dried to remove liquid and weighted. Throughout the entire process, fresh protease solution was regularly replaced to ensure that the enzyme activity was maintained at the ideal level during the degradation process. The experiment was repeated for the films placed in a PBS buffer solution as the control group.

2.2.8. Cytotoxicity and biocompatibility

Mouse fibroblasts (L929) were used to evaluate the biocompatibility of silk fibroin films. Before the cell experiment, silk films were cut into discs of appropriate size. In order to sterilize the films, they were first placed under a UV light for two hours and then soaked in 70% ethanol. After rinsing three times with PBS to completely remove the ethanol, the samples were placed in a 96-well plate. Then take out the pre-incubated dishes, digest the adherent cells with trypsin, remove the trypsin, suspend the L929 cells in new Dulbecco's modified Eagle medium (DMEM) at 104 cells/cm^3, and add 10 %(v/v) of fetal bovine serum. L929 cells were seeded on silk fibroin membrane, placed in a cell culture incubator at 37 °C and 5% CO_2, and passed MTT (3-[4,5-dimethylthiazole-2]- 2,5-diphenyl Tetrazolium bromide) method to evaluate the cell viability of different scaffolds. After the cells were incubated on the membrane for 1, 3, and 5 days, the supernatant was removed, washed twice with PBS, and 200 μl of 0.5 mg/ml MTT solution was added. After incubating for 4 h in the incubator, the supernatant was removed. Replace the MTT solution with 200 μl of DMSO and shake for 10 min at room temperature to completely dissolve the crystals formed by formazan, then measure the UV absorbance at 490 nm on the BioTek immunoassay analyzer (EL-x800), and set three parallel samples. Take the average value, set up a group of cell control groups without material, and calculate the cell viability with the following equation (6) [12–13]:

$$Viability = \frac{D_s}{D_c} \times 100\% \tag{6}$$

where D_s is the absorbance of the stent and D_c is the absorbance of the control.

2.2.9. Breathability analysis

The gas permeability (breathability) analysis of SF film under different thicknesses was performed through a Capillary Flow Porometer (CFP, ipore-1500AEX-Clamp, Porous Materials, Inc., USA) and the mass change of silica gel in glass bottle, respectively. Different sample solutions were cast to form films with 0.4 mm and 0.8 mm thicknesses, and then cut into a same 2 × 1.5 cm^2 area, and tested at 25 ℃, 70 KPa pressure and in nitrogen atmosphere. The gas permeability P (m^3Â·m^{-2}Â·h^{-1}Â·kPa^{-1}) of the films can be calculated according to equation (7):

$$P = \frac{Q}{\Delta p \hat{A} \cdot A} \tag{7}$$

where Q is the gas flow rate at each pressure, Δp is the transmembrane pressure difference, and A is the membrane area. At least three measurements were taken for each sample.

3. Results and discussion

3.1. Surface morphology

The morphology of regenerated silk films treated with different ultrasonic treatments were observed by scanning electron microscopy (SEM), as shown in Fig. 1b. Films treated with different time periods showed different morphology at the surface level (Fig. 1b, MSF ~ MSFT-30). The films without ultrasound showed uniform particle connectors at the scale of 1 μm (Fig. 1b, MSF), and the local magnified image at the scale of 50 nm also clearly showed nanoparticles (Fig. 1b(I)), which was consistent with results in the previous studies [4,13,32]. Films treated with 600 W for 1 and 5 min began to show stripe projection, and the particles began to grow swelling with a local agglomeration and bulge (Fig. 1b, MSFT-1, MSFT-5), while the local magnified images with a 10^5 magnification (50 nm scale bar) showed that more tiny holes and gaps appeared among nanoparticles compared to that of without ultrasound (Fig. 1b(II), 1b(III)). After the 15 mins treatment, the particles on the film surface were loosely distributed with more cracked with island-like structures (Fig. 1b, MSFT-15). Ultrasound treatment that lasted for 30 min (Fig. 1b, MSFT-30) caused the cracks to become larger, while the local particle size seemed smaller than that of 15 mins samples (Fig. 1b (IV)). For all film treated with different ultrasonic intensity during 30 mins, their apparent characteristics are also different (Fig. 1b, MSFP-100 ~ MSFP-800). As the ultrasonic intensity gradually increased, the film treated with 100 W began to show local continuous convex and smooth planes, and the film treated with an intensity of 300 W developed agglomeration and projection among particles. The film treated with 500 W was closely arranged with particles and appeared cracks like island, while the film treated with 700 W and 800 W showed relatively uniform particle distribution. At the scale of 50 nm bar, all films showed different distribution of nanoparticles, with tiny holes or gaps between them (Fig. 1b(VI) ~ 1b(X)). From these images, it was possible to find the effect of various ultrasonic powers on the topology of the SF films. Simultaneously, it also indicated that the ultrasound could reduce the agglomeration of the fibers, distribute them evenly throughout the silk

matrix, and increase the gaps between nanoparticles.

3.2. Structural analysis

Fourier transform infrared spectroscopy (FTIR) is a powerful method to analyze the secondary structure of proteins (Figure S1) [27]. In general, the spectral region of 1700–1500 cm^{-1} is the absorption region of Amide I and Amide II groups [4,7,32–34], while the Amide III region is from 1350 to 1200 cm^{-1}. The N–H stretching vibration of silk protein is shown in the Amide N region (3310 ~ 3270 cm^{-1}) which is a part of the Fermi resonance doublet and is connected with its second component, Amide N′ (3100 ~ 3030 cm^{-1}) [33–35]. Among the listed regions, the Amide I region is the most commonly used region for quantitative analysis of secondary protein structure [1,33]. For regenerated MSF films obtained by using ultrasonic treatment of different time or power, the characteristic peaks of the infrared spectrum of the samples shifted with the extension of ultrasonic time or intensity (Fig. 1c). Specifically, for ultrasound times of 0 min to 30 mins, the peak of 1649 cm^{-1} gradually moved to 1647 cm^{-1}, 1538 cm^{-1} to 1544 cm^{-1}, and 1250 cm^{-1} to 1255 cm^{-1}, as well as 2931 cm^{-1} to 2945 cm^{-1} and 3271 cm^{-1} to 3269 cm^{-1}(Figure S1) . Similarly, for different ultrasonic power treated MSF samples, when power increased from 100 W to 800 W, the peak gradually shifted from 1649 cm^{-1} to 1639 cm^{-1}, 1538 cm^{-1} to 1532 cm^{-1}, 1250 cm^{-1} to 1246 cm^{-1}, 3234 cm^{-1} to 3227 cm^{-1} (Figure S1a). Moreover, all peak widths in Amides I, II and III were significantly increased after the ultrasound treatment, which indicates the partial transition of intermediate silk I structure to β-sheet crystal dominated silk II structure occurred for ultrasound treated samples (Fig. 1c).

In order to further understand the effects of different ultrasonic time and intensity on the secondary conformation content of protein, peaks curve-fittings in the Amide I region were carried out (Figure S1c), and results are shown in Table S1 [27]. The fitted individual peaks can be assigned as side chains (S), intermolecular β-sheets (B^{er}), intramolecular β-sheets (B^{ra}), random coils (R), α-helix (A) and β-turns (T), as we described previously [4,27]. It was found that as the ultrasonic treatment time increased, the total β-sheet content (sum of the intermolecular (B^{er}) and intramolecular β-sheets (B^{ra})) increased gradually from 13.41% for MSFT-1 sample to 18.68% for MSFT-30 sample, while random coils decreased from 39.33% for MSFT-1 sample to 34.06% for MSFT-30 sample (Fig. 1d). For the silk fibroin samples treated with different ultrasonic power, their secondary structures also showed the same trend of change. With the power increasing from 100w to 800w, the total β-sheet content increased from 17.39% to 20.52%, while the random coils decreased from 35.85% to 31.45% (Fig. 1d). However, we also found that with the increase of the ultrasound time or power, the intramolecular β-sheet content decreased, while both the intermolecular β-sheet and α-helix contents increased (Table S1).

It should be noted here that the total β-sheet content measured after the film fabrication is not the maximum β-sheet crystallinity that can be obtained from the silk film. Through additional treatments, such as long-term (>1h) annealing in water or methanol, the secondary structure of the ultrasonic silk films may be completely different. Figure S2 and Table S2 respectively demonstrated the FTIR spectra and the calculated secondary structure percentages of the sonicated SF films annealed in water for 1 h. The results showed that for all silk films, a greater total β-sheet content (>50%) can be obtained. However, due to this additional annealing treatment, the secondary structure change trend of the samples caused by the increase in the ultrasound time or power is no longer obvious.

XRD is then used to study the crystallinity of silk fibroin [35]. The main structure of Silk I conformation includes ordered α-helix and coils, with diffraction angles that appear at 24.7°, 28.2° and 27.9°. The Silk II structure is mainly β-sheet structures which corresponds to peaks around 20.4°, 24.1°, 25.6° and 30.9° [23,35–38]. Fig. 1e showed that the diffraction peak of untreated silk sample (MSF) is at 24.7° and 28.2°, indicating a Silk I structure, As the ultrasonic time increased (1 min ~ 30 mins), the peak was widened (MSFT-1 ~ MSFT-30), and a new peak at 24.1° (MSFT-30) appeared which implied the existence of Silk II (β-sheet crystalline) structure [23]. Meanwhile, besides two peaks around 24.1° and 25.6°, another shoulder peak at 20.4° was also shown for samples treated with 100 W to 800 W ultrasound (MSFP-100 ~ MSFP-800), respectively (Figure S3a). The contents of Silk I and Silk II structure of all SF films were calculated by a Gaussian fitting method (Figure S3b), and summarized in Table S3, which showed that Silk I content decreased while Silk II structure (β-sheet crystalline) increased with the enhanced of ultrasonic effect (time and intensity) (Fig. 1f). These results were similar with those from FTIR calculation (Fig. 1d, total β-sheets in Table S1). Wu *et al.* [39] demonstrated that the random coils or β-turns structure in silk fibroin protein can be transformed into α-helix structure during ultrasound treatment, and then the unstable α-helix structure could easily be transformed into β-sheet structure due to hydrogen bonding. Zheng *et al.* [40] also confirmed that the conformation of silk fibroin would undergo transformation with the increase of ultrasonic power. Besides, some studies [41–43] also proved that the long-time sonication could make the random coils converted to stable β-sheet structures and accelerate the formation of silk fibroin gels. Therefore, ultrasound time and power can precisely regulate the secondary structures and the crystallinities of silk fibroin materials.

3.3. Thermal analysis

Thermal analysis (Fig. 2) is one of the most important techniques to characterize the macroscopic physical properties of materials due to its ability to reveal the microphase structures for various materials [44]. Fig. 2a showed the standard DSC curves of silk samples treated by using 600 W ultrasound for 0 min (MSF) ~ 30 mins (MSFT-30). And the DSC curves of samples under 100 W (MSFP-100) ~ 800 W (MSFP-800) ultrasonic power for 30mins were showed in Figure S3c. Three thermal events appeared in all samples: the dehydration from ambient temperature to 100 ℃, glass transition at a range of 150 ℃ to 250 ℃ and the decomposition after 250 ℃ [45–46]. All samples treated with different times showed a small dehydration peak in DSC curves while those treated with different power intensities were inconspicuous, which implied that under the same condition, the change of ultrasonic power had a greater effect on the bound-water content of the films when compared to the changes due to the length of ultrasonic treatment. Meanwhile, DSC results showed that the decomposition of endothermic peaks of all the samples treated by ultrasound were shifted slightly to a higher temperature ($T_{DSC\text{-}p}$, Fig. 2a). To further understand the glass transformation process of the samples, modulating StepScan DSC was carried out [44–45] for all silk films. The modulating DSC profiles of silk protein with different ultrasonic time were shown in Fig. 2b. With the increase of ultrasonic time, the glass transition temperature and specific heat increment of silk fibroin samples decreased, which suggested that ultrasound could raise the mobility of silk fibroin chains (T_g, Table 1). The same phenomenon also appeared on those samples treated with different intensity (Figure S3d).

The thermogravimetric analysis (TGA) of the samples treated with different ultrasonic time also showed that the samples had been dehydrated around 100℃ while the molecular chain started to break around 300 ℃ which resulted in a decomposition reaction (Fig. 2c). The inserted DTG curve showed the rate of decomposition for each corresponding sample. T_p temperature on DTG (Fig. 2ć inserted in Fig. 2c) represents the temperature corresponding to the maximum weight loss rate of the sample. Fig. 2d demonstrated the changing trend of T_g, $T_{DSC\text{-}p}$ and T_p under different ultrasonic time and power. It can be found that at T_p temperature decreased slightly with the increase of ultrasonic time or ultrasonic power (Fig. 2d). And the residual mass at 400 ℃ of the sample with longer ultrasonic time or with bigger power intensity is slightly higher ($Y_{r=400}$/%, Table 1).

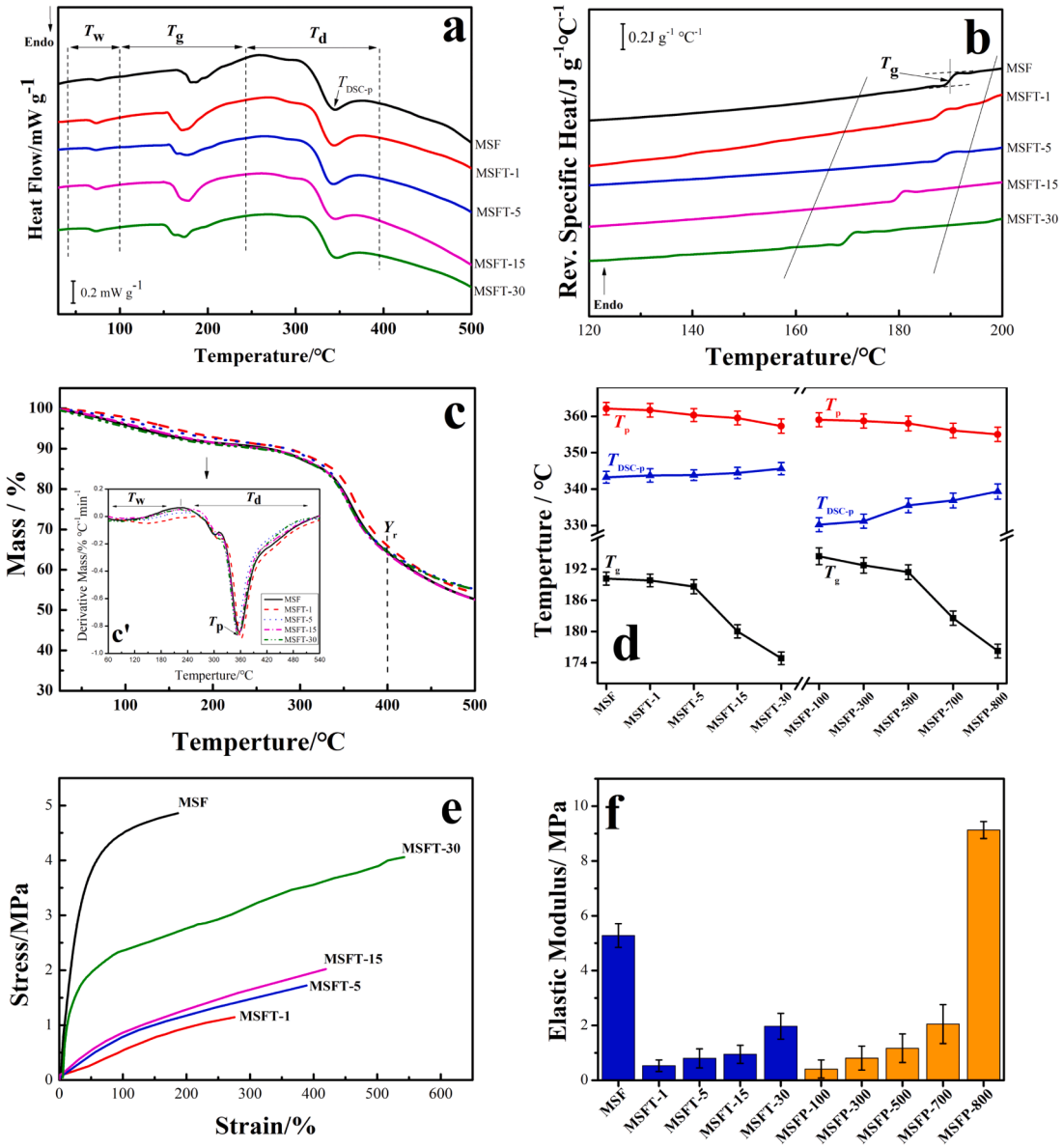

Fig. 2. (a) Standard DSC curves of silk fibroin films with different ultrasonic time (0 ~ 30 mins). T_w, T_g and T_d represented the dehydration, glass transition and decomposition regions in standard DSC curve, respectively. (b) Reversing heat capacity measured from the modulating Step-Scan DSC curves of the samples with different ultrasonic time (0 ~ 30 mins). (c) TG and DTG (inserted figure c') analysis of SF films under different ultrasonic treatment (0 ~ 30 mins). (d) The changing trend of T_g, T_{DSC-p} and T_p of different SF films. T_g and T_{DSC-p} represented glass transition temperature and decomposition peak temperature from DSC measurement, and T_p is the temperature at the maximum weight loss rate of the sample from DTG curve. (e) Stress–strain curves of SF films under different ultrasonic treatment (0 ~ 30 mins). (f) Elastic modulus of SF films as a function of ultrasonic time (0 ~ 30 mins; MSF, MSFT-1, MSFT-5, MSFT-15 and MSFT-30) and ultrasonic intensity (100 ~ 800 W; MSFP-100, MSFP-300, MSFP-500, MSFP-700 and MSFP-800). Each sample was immersed in water for 20 min prior to DMA testing.

3.4. Mechanical properties

Fig. 2e shows the tensile stress–strain curves of the regenerated silk fibroin films after ultrasonic processing. To mimic the typical water-swelling condition in a biological environment, all samples were first immersed in deionized water at 37 ℃ for 20 min before the DMA test. The elongation of silk fibroin films with ultrasonic treatment was significantly improved (Fig. 2e, curve MSFT-1 ~ MSFT-30) when compared with the untreated film (Fig. 2e, curve MSF). The elongation ratio of silk fibroin membrane treated with the 600 W ultrasound was about 1.5 times (MSFT-1), 2.1 times (MSFT-5), 2.3 times (MSFT-15) and 2.9 times (MSFT-30) to the elongation ratio of non-ultrasound sample, respectively (calculated from Table 1). When compared with the untreated sample (MSF), the elastic modulus of ultrasound treated samples (MSF-1, MSF-5, MSF-15, MSF-30) are smaller. However, the elastic modulus and the extension strength of treated silk fibroin films increased with the increase of ultrasonic time (Table 1), such as the elastic modulus increasing from 0.53 ± 0.21 MPa for MSFT-1 to 1.97 ± 0.47 MPa for MSFT-30 (Table 1). Simultaneously, silk fibroin films under different ultrasonic intensities also showed the similar tendency (Figure S4). As the ultrasonic intensity increase, the elastic modulus of the films also increased, from 0.08 ± 1.21 for MSFP-100 to 9.13 ± 0.31 for MSFP-800 (Table 1). The histogram of young's modulus of all samples clearly shows the influence of ultrasound on the elastic properties of the samples (Fig. 2f). After ultrasonic treatment, the breaking strength and elongation of silk films were all significantly improved except for the MSFP-800 sample. The strength of extension of the 800 W treated sample was the largest among all the samples (19.13 ± 1.93 MPa), but

Table 1
Thermal and mechanical properties of ultrasound treated silk fibroin films obtained from DSC, TG and DMA measurements*.

Sample	Time/min or Intensity/W	T_g /℃	ΔC_p /J·℃$^{-1}$	$T_{DSC\text{-}d}$ /℃	$Y_{r=400}$ /%	Elastic modulus /MPa	Strength of extension /MPa	Elongation /%
MSF	$0^{t,I}$	190.17 ± 0.21	0.91 ±0.07	343.27 ± 1.11	63.94 ±0.17	5.28 ±1.43	4.86 ±0.34	186.64 ±1.20
MSFT-1	1^{t}	189.81 ± 0.52	0.60 ±0.06	343.76 ± 1.02	63.98 ±0.19	0.53 ±0.21	1.14 ±0.12	275.39 ±2.41
MSFT-5	5^{t}	188.62 ± 0.54	0.60 ±0.07	343.85 ± 1.16	64.42 ±0.16	0.80 ±0.35	1.72 ±0.21	388.93 ±3.71
MSFT-15	15^{t}	180.01 ± 0.63	0.59 ±0.10	344.45 ± 1.38	64.56 ±0.18	0.95 ±0.33	2.02 ±0.43	419.16 ±4.24
MSFT-30	30^{t}	174.84 ± 0.72	0.43 ±0.11	345.63 ± 1.45	64.79 ±0.11	1.97 ±0.47	4.06 ±0.72	542.36 ±1.33
MSFP-100	100^{I}	194.47 ± 0.61	0.74 ±0.08	330.21 ± 1.33	62.27 ±0.12	0.08 ±1.21	0.26 ± 0.53	362.13 ±0.75
MSFP-300	300^{I}	192.72 ± 0.64	0.67 ±0.07	331.19 ± 1.52	62.71 ±0.17	0.81 ±0.44	1.22 ± 0.66	234.72 ±0.22
MSFP-500	500^{I}	191.42 ± 0.52	1.08 ±0.04	335.51 ± 1.51	62.74 ±0.14	1.17 ±0.52	2.25 ± 0.34	212.34 ±0.27
MSFP-700	700^{I}	182.56 ± 0.47	0.65 ±0.06	336.88 ± 1.47	63.67 ±0.13	2.05 ±0.71	2.56 ± 0.27	237.13 ±0.16
MSFP-800	800^{I}	176.24 ± 0.59	0.63 ±0.11	339.35 ± 1.42	64.08 ±0.16	9.13 ±0.31	19.13 ± 1.93	25.91 ±0.12

* Superscripts *t* and *I* represent ultrasonic time and ultrasonic intensity, respectively. T_g, ΔC_p and $T_{DSC\text{-}d}$ were derived from the glass transition temperature, specific heat increment and decomposition peak temperature on the DSC curves, respectively. $Y_{r=400}$ denoted the mass residual amount of the sample at 400℃ on the TG curve. The elastic modulus, strength of extension and elongation were obtained from DMA measurements; Each sample was tested at least 5 times.

with the smallest elongation of 25.91 ± 0.12 %. Generally, the strength and elongation rate for each material is contradictory. If a material is more rigid (strength), then the sample will have poorer ductility (elongation ratio) [47]. However, in this work, for treated samples only, both of the values can increase together by increasing ultrasonic time or intensity. It is well known that the elongation at break was determined by the alignment of protein molecular chains [4,8,48–51]. Therefore, there could be two reasons for this phenomenon: (1) ultrasound helped a part of the noncrystalline region of SF chains form a more ordered orientation; and (2) the water molecules had a stronger plasticizing effect on the silk fibroin molecular chains during the ultrasound treatment [47–50]. After drying and soaking in water, the silk molecular chains were aligned [49–50], which allowed for the intermolecular β-sheets to form that promoted materials strength and flexibility. Therefore, with the increase of the ultrasound time or power, both the ductility and rigidity of silk fibroin films can be greatly improved.

3.5. Biological properties

In addition, the effects of ultrasound on the material's biological properties, including hydrophilicity, enzymatic degradability and biocompatibility were further investigated (Fig. 3). First, the water contact angle was measured, which is an important parameter that affects the adhesion, proliferation, migration and viability of cells. The water contact angle decreased from 95.92° to 66.40° with the ultrasonic time increasing from 0 min to 30 mins, and the angle also decreased from 87.76° for the 100 W intensity to 67.37° for the 800 W intensity ultrasonic power (Fig. 3a). The pure SF film has a hydrophobic property due to its carboxyl group, amine group, hydroxyl group and three-dimensional nanofibrous structure [52]. After ultrasound treatment, more hydrophilic chain segments were presented to the material surface [52–53]. Wang *et al.* [53] also found that the ultrasonic treatment can cause the realignment of the protein molecules and improve their hydrophilicity and thermal stability of silk fibroin. Therefore, more hydrophilic interaction between molecular chains could be exhibited. Hence, the results suggested that the ultrasound-treated SF films became more hydrophilic with the increase of treatment time and power.

The degradation study of silk films in proteinase K solution showed that as ultrasonic treatment power increased, the rate of degradation also increased (Fig. 3b). While their degradation in deionized water and in PBS buffer solution exhibit very low degradation and their weight remained fairly stable over the time (Figure S5). The apparent morphology, microstructure and molecular weight of the membrane samples could also directly affect the enzymatic degradation rate. After 6 h, the total mass losses of films treated at 100–800 W power were measured to be about 20、30.2、31.6、35.3 and 40%, respectively. After 24 h, the masses continued to degrade and demonstrated a relatively high level of degradation. At 72 h, their remaining masses reduced to 58.6% for MSF, 40.5% for MSFP-100, 38.5% for MSFP-300, 35.9% for MSFP-500, 30.4% for MSFP-700 and 25.7% for MSFP-800 of the original mass, respectively. The enzymes degradation rate of film that weren't treated with ultrasound was the slowest among all samples. The samples treated with ultrasonic time under the same power also showed the same degradation trend in enzyme protein solution (Fig. 3c). With the extension of ultrasonic time, the degradation rate of film in the enzyme increased [54–56]. At 72 h, their remaining masses reduced to 52.9% for MSFT-1, 48.4% for MSFT-5, 44.9% for MSFT-15, and 39.1% for MSFT-30 of the original mass, respectively. Mi *et al.* [54] produced chitin/poly(D,L-lactide-co-glycolide) composite microspheres as a drug-delivery system. They found that the amorphous structure of the blends allowed rapid water penetration. Numerous studies [9,54–59] also demonstrated that enzymatic biodegradation process and biostability of biopolymer materials are comparatively complicated, which could be associated with the structure, the surface morphology, and the molecular interaction between polymer chains. During the ultrasound treatments, both the hydrophilicity and the molecular arrangement of the silk films were significantly improved, which may contribute to the faster degradation of the material.

Films treated with ultrasound for 1 ~ 30 min, as well as those treated with ultrasound at 100 ~ 800 W, were selected for the cell biocompatibility and viability test (Fig. 3d). The results illustrated that>80% of the cells in all samples survived during the culture time. Simultaneously, the cells survival rate and proliferation rate of all samples increased with increased culture times. For example, the cell survival rate of MSF-30 samples was 95% at 24 h of incubation and 107% and 114% at 48 and 72 h, respectively. These results indicated that the ultrasound-treated films can provide a favorable environment for cells attachment and proliferation. After incubation for 24 h, the cell viabilities (111%-131%) in the films treated with ultrasound (MSFT and MSFP) were higher than that treated without ultrasound (MSF, 105%). The trend at

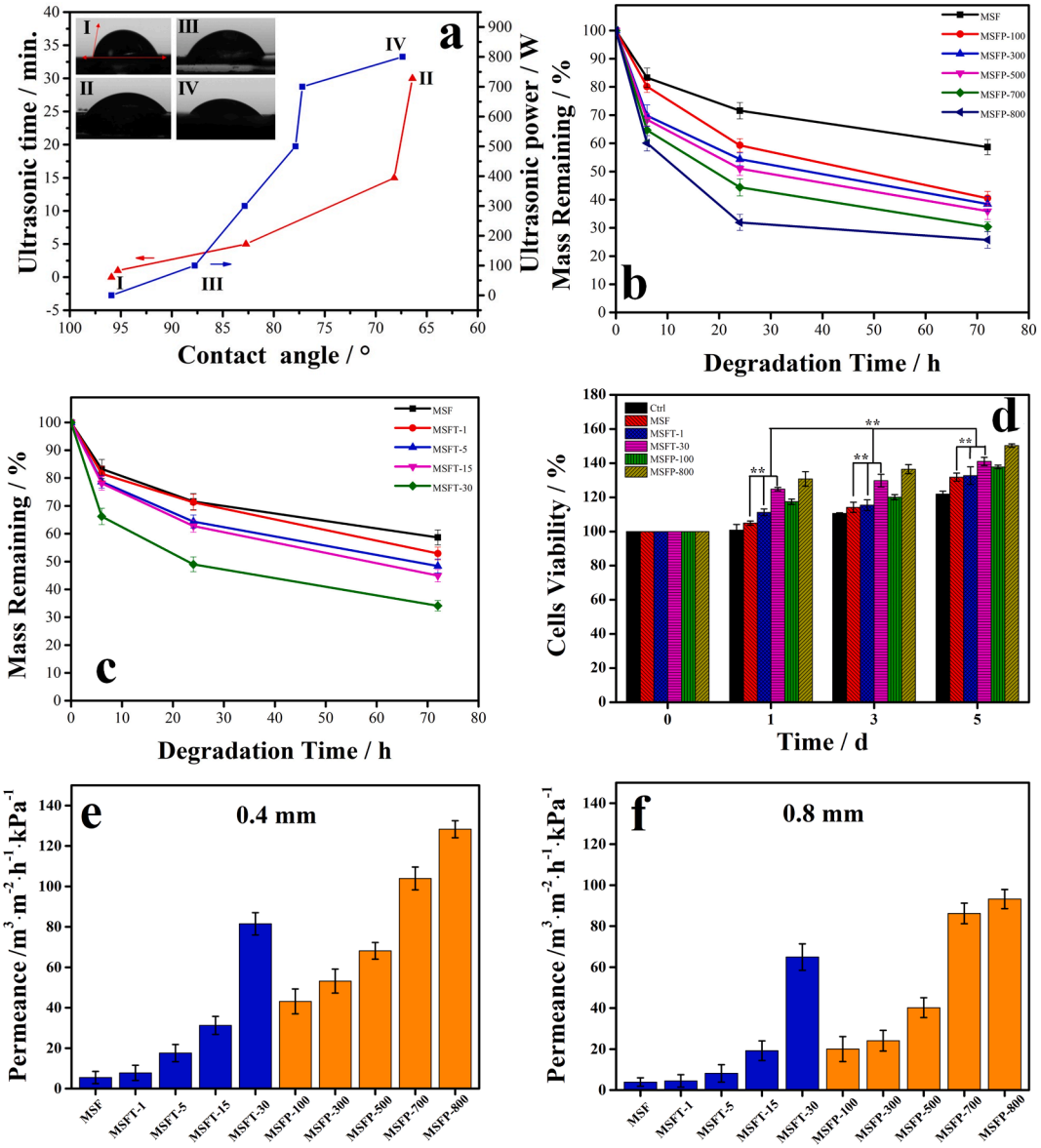

Fig. 3. ga) Water contact angle of SF films ultrasonically treated with different time from (I) 0 min to (II) 30 mins at 600 W, and under different intensity from (III) 100 W to (IV) 800 W for 30 mins, respectively. Protease XIV enzymatic degradation profiles of (b) MSF, MSFP-100, MSFP-300, MSFP-500, MSFP-700 and MSFP-800, and (c) MSF, MSFT-1, MSFT-5, MSFT-15 and MSFT-30 film samples. (d) The mouse fibroblast cell (L929) viability after 0, 1, 3, 5 days, on the surfaces of MSF, MSFT-1, MSFT-30 and MSFP-100 and MSFP-800 samples using a glass surface as the control (** $p < 0.01$). The breathability of ultrasound treated SF films with (e) 0.4 mm, and (f) 0.8 mm thickness, measured at 25 ℃, 70 KPa pressure and nitrogen atmosphere.

48 h and 72 h was similar to that at 24 h. Moreover, the films treated with longer ultrasonic time (MSFT-30) or higher ultrasonic intensity (MSFP-800) possessed more cell adhesion and growth. The cell growth viability reached 150% on the film treated for 30 min and 800 W ultrasound, which demonstrated that appropriate ultrasonic treatment material was more conducive to cell adhesion and growth. We have discussed that different surface micro-patterns could manipulate cells growth and proliferation on biopolymer blend films [59]. Dong *et al.* [60] also investigated the growth of cells on the zein protein films, and found that the cell adhesion was improved as the surface particle size decreased. Zhang *et al.* [61] revealed that the behavior of cell attachment and proliferation mostly depended on the material surface characteristics, include the hydrophily. Our experiment results also proved the feasibility of using the tunable microstructure of the ultrasound-controlled silk protein materials as substrates for cell culture in biomedical field.

The breathability analysis results of SF films also showed significant differences. For the 0.4 mm film samples (Fig. 3e), as the ultrasound time increased from 1 min to 30 mins, the air permeability increased from 7.79 ± 3.78 to 81.49 ± 5.53 $m^3 \cdot m^{-2} \cdot h^{-1} \cdot kPa^{-1}$. For the 0.8 mm film samples (Fig. 3f), the increasing trend is the same (Table S4). Similar phenomena were also observed for samples treated with different ultrasonic intensities (Fig. 3e, 3f and Table S4). Therefore, the air permeability of the SF film can be greatly improved by increasing the ultrasonic treatment time or intensity, and reduced by increasing the film thickness. This may be due to the formation of unique silk nanostructures during the ultrasound treatments, as shown by the SEM study.

3.6. Mechanism of ultrasound on silk material

Based on the above results, we envision the following mechanistic (Fig. 4) understanding of the effect of ultrasound on the structural, thermal, mechanical and biological properties of silk fibroin materials fabricated from the FA-$CaCl_2$ solution (Fig. 4a). Generally, the *Bombyx*

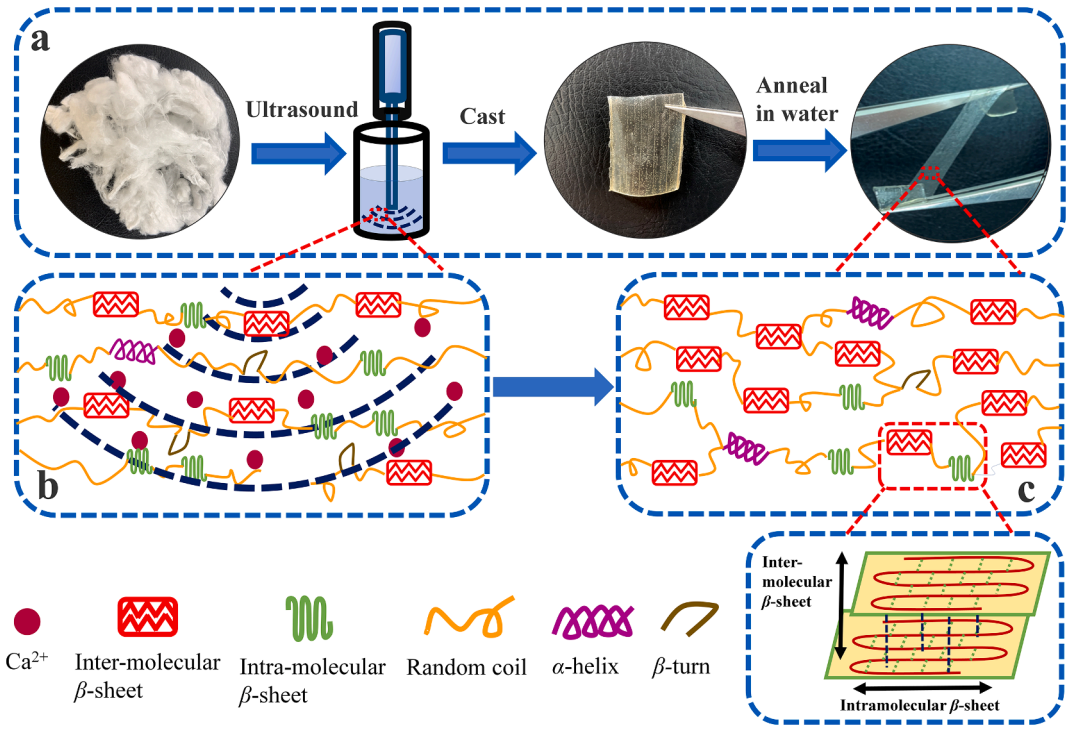

Fig. 4. The mechanism of ultrasonic treatments on silk fibroin materials regenerated from the formic acid-$CaCl_2$ solution system.

mori silk fibroin protein is composed of three proteinaceous components: a heavy chain (H-chain, ca. 350 kDa) contained alternating hydrophobic and hydrophilic regions; a light chain (L-chain, ca. 25 kDa) possessed more hydrophilicity and linked to H-chain via disulfide bonds; and a small glycoprotein P25 protein (of ca. 30 kDa) that maintained the integrity of the complex through non-covalent hydrophobic interactions with the H-chain and L-chain [1,62]. Based on the theoretical hydrophobicity map of the H-chain in the SF [62], a large number of hydrophobic amino acid residues, such as the blocks of $(Gly\text{-}Ala\text{-}Gly\text{-}Ala\text{-}Gly\text{-}Ser)_n$, can promote the self-assembly of SF molecules. During this period, the H-chain can undergo a significant conformational transition in the solution state [62]. Under the mechanical shear and heat transfer promoted by ultrasound, the agglomeration of SF molecules and the self-assembly of the protein micellar system can be further enhanced by hydrophobic interactions [62]. Previous studies [4] have showed that the FA-$CaCl_2$ solvent system was able to turn the stacked β-sheet crystals in silk fibroin fibers into single-layer intramolecular β-sheets or random coils in the solution [4,13,32]. In this work, it was found that ultrasound treatment could evenly distribute the calcium ions throughout the solution system (Fig. 4b), and enhance the penetration of calcium ions into the silk structure. Ultrasound also stretched the silk molecular chain segments, making the chain segment rearrange in a more orderly fashion as intermolecular β-sheets and α-helix increased, while random coils and β-turns decreased in the silk fibroin structure (Fig. 4c). The increase in intermolecular β-sheets and α-helix contents caused the silk to be insoluble in water with both mechanical strength and flexibility (Fig. 4c). In addition, ultrasound also increased the gap between the molecular chain segments and exposed more hydrophilic groups. These structures enhanced gas permeability of the samples, and promoted cell adhesion, differentiation and growth within samples such as MSFT-30 and MSFP-800. Overall, our results suggested that the ultrasonic treatment in FA-$CaCl_2$ solution greatly improved various physical properties and biological responses when compared to untreated films.

4. Conclusions

This study presented a mechanism study on the structural transformation and physical and biological properties of regenerated *Bombyx Mori* silk fibroin films under various ultrasonic treatments. The study revealed that the intensity and action time of ultrasonic treatment could facilitate the self-assembly of silk molecules, and enhance the interactions between calcium ions and silk molecular chains, which promoted the formation of β-sheets crystals. With the increase of ultrasonic intensity or the prolongation of time, the intermolecular β-sheets and α-helix structures increased, which caused the silk films to be insoluble in water with enhanced mechanical strength and flexibility. Simultaneously, their glass transition temperature and the specific heat increment decreased, and possessed a good thermal stability with a tunable enzymatic degradation rate. Importantly, we have found that high-intensity and longer ultrasonic treatment enable silk fibroin film to obtain better hydrophilic swelling performance, higher breathability and greater cell compatibility, due to the increase of hydrophilicity and intermolecular interactions in SF films. With these results, a model was proposed to explain the mechanism of ultrasonic treatments on the SF films. This study offered an important strategy on how to physically manipulate the structure of silk-based biomaterials in order to tune its properties by simply using ultrasound. These properties can be applied to the fields of biomedicine and sustainable materials, such as air or chemical filters, controlled drug delivery systems, and wound dressings or artificial tissues that provide unique biocompatibility and excellent mechanical strength and flexibility.

CRediT authorship contribution statement

Bowen Cai: Data curation, Formal analysis, Investigation, Writing – original draft. **Hanling Gu:** Investigation, Writing – original draft. **Fang Wang:** Conceptualization, Supervision, Funding acquisition, Writing – review & editing. **Kyle Printon:** Writing – review & editing. **Zhenggui Gu:** Resources. **Xiao Hu:** Conceptualization, Funding acquisition, Writing – review & editing.

Declaration of Competing Interest

The authors declare that they have no known competing financial

interests or personal relationships that could have appeared to influence the work reported in this paper.

Acknowledgements

This study is supported by the National Natural Science Foundation of China (21973045). K.P. and X.H. are supported by Rowan University Seed Research Grants and the US NSF Biomaterials Program (DMR-1809541).

Appendix A. Supplementary data

Supplementary data to this article can be found online at https://doi.org/10.1016/j.ultsonch.2021.105800.

References:

[1] J.G. Hardy, T.R. Scheibel, Composite materials based on silk proteins, Prog. Polym. Sci. 35 (9) (2010) 1093–1115.
[2] T.H. Mokhothu, M.J. John, Review on hygroscopic aging of cellulose fibres and their biocomposites, Carbohydr. Polym. 131 (2015) 337–354.
[3] Y.u. Wang, J. Guan, N. Hawkins, D. Porter, Z. Shao, Understanding the variability of properties in Antheraea pernyi silk fibres, Soft Matter 10 (33) (2014) 6321–6331.
[4] Y. Xue, F. Wang, M. Torculas, S. Lofland, X. Hu, Formic Acid Regenerated Mori, Tussah, Eri, Thai, and Muga Silk Materials: Mechanism of Self-Assembly, ACS Biomater. Sci. Eng. 5 (12) (2019) 6361–6373.
[5] G.H. Altman, F. Diaz, C. Jakuba, T. Calabro, R.L. Horan, J. Chen, H. Lu, J. Richmond, D.L. Kaplan, Silk-based biomaterials, Biomaterials 24 (3) (2003) 401–416.
[6] V.J. Neubauer, A. Döbl, T. Scheibel, Silk-Based Materials for Hard Tissue Engineering, Materials 14 (3) (2021) 674.
[7] P. Cebe, B.P. Partlow, D.L. Kaplan, A. Wurm, E. Zhuravlev, C. Schick, Silk I and Silk II studied by fast scanning calorimetry, Acta Biomater. 55 (2017) 323–332.
[8] Q.C. Liu, F. Wang, Z.Z. Gu, Q.Y. Ma, X. Hu, Exploring the Structural Transformation Mechanism of Chinese and Thailand Silk Fibroin Fibers and Formic-Acid Fabricated Silk Films, Int. J. Mol. Sci. 19 (11) (2018) 3309.
[9] E.M. Pritchard, P.B. Dennis, F. Omenetto, R.R. Naik, D.L. Kaplan, Physical and chemical aspects of stabilization of compounds in silk, Biopolymers 97 (6) (2012) 479–498.
[10] L.-D. Koh, Y. Cheng, C.-P. Teng, Y.-W. Khin, X.-J. Loh, S.-Y. Tee, M. Low, E. Ye, H.-D. Yu, Y.-W. Zhang, M.-Y. Han, Structures, mechanical properties and applications of silk fibroin materials, Prog. Polym. Sci. 46 (2015) 86–110.
[11] X. Hu, K. Shmelev, L. Sun, E.-S. Gil, S.-H. Park, P. Cebe, D.L. Kaplan, Regulation of Silk Material Structure by Temperature-Controlled Water Vapor Annealing, Biomacromolecules 12 (5) (2011) 1686–1696.
[12] X. Zhang, L. Xiao, Z. Ding, Q. Lu, D.L. Kaplan, Fragile-Tough Mechanical Reversion of Silk Materials via Tuning Supramolecular Assembly, ACS Biomater. Sci. Eng. 7 (6) (2021) 2337–2345.
[13] F. Zhang, X. You, H. Dou, Z. Liu, B. Zuo, X. Zhang, Facile fabrication of robust silk nanofibril films via direct dissolution of silk in CaCl2-formic acid solution, ACS Appl. Mater. Interfaces 7 (5) (2015) 3352–3361.
[14] X.-G. Li, L.-Y. Wu, M.-R. Huang, H.-L. Shao, X.-C. Hu, Conformational transition and liquid crystalline state of regenerated silk fibroin in water, Biopolymers 89 (6) (2008) 497–505.
[15] B. Rokita, J.M. Rosiak, P. Ulanski, Ultrasound-Induced Cross-Linking and Formation of Macroscopic Covalent Hydrogels in Aqueous Polymer and Monomer Solutions, Macromolecules 42 (9) (2009) 3269–3274.
[16] G. Carissimi A.A. Lozano-Pérez M.G. Montalbán S.D. Aznar-Cervantes J.L. Cenis G. Víllora Revealing the Influence of the Degumming Process in the Properties of Silk Fibroin Nanoparticles J. Polymers 11 12 (2019) 2045. 2045 10.3390/polym11122045.
[17] C.W. Wong, Y.S. Chan, J. Jeevanandam, K. Pal, M. Bechelany, M. Abd Elkodous, G. S. El-Sayyad, Response Surface Methodology Optimization of Mono-dispersed MgO Nanoparticles Fabricated by Ultrasonic-Assisted Sol-Gel Method for Outstanding Antimicrobial and Antibiofilm Activities, J. Cluster Sci. 31 (2) (2020) 367–389.
[18] Y.i. Pan, C.J. Hurren, Q. Li, Effect of sonochemical scouring on the surface morphologies, mechanical properties, and dyeing abilities of wool fibres, Ultrason. Sonochem. 41 (2018) 227–233.
[19] P. Cass, W. Knower, E. Pereeia, N.P. Holmes, T. Hughes, Preparation of hydrogels via ultrasonic polymerization, Ultrason. Sonochem. 17 (2) (2010) 326–332.
[20] S. Mohamadi Saani, J. Abdolalizadeh, S. Zeinali Heris, Ultrasonic/sonochemical synthesis and evaluation of nanostructured oil in water emulsions for topical delivery of protein drugs, Ultrason. Sonochem. 55 (2019) 86–95.
[21] K.G. Akpomie, J. Conradie, Biogenic and chemically synthesized Solanum tuberosum peel–silver nanoparticle hybrid for the ultrasonic aided adsorption of bromophenol blue dye, Sci. Rep. 10 (1) (2020) 17094.
[22] A.I. Susanin, E.S. Sashina, V.V. Zakharov, M. Zaborski, D.A. Kashirskii, Conformational Transitions of Silk Fibroin in Solutions under the Action of Ultrasound, Russ. J. Appl. Chem. 91 (7) (2018) 1193–1197.
[23] Z.Y. Li, J.Y. Wang, B.D. Zheng, Z.B. Guo, Impact of combined ultrasound-microwave treatment on structural and functional properties of golden threadfin bream (Nemipterus virgatus) myofibrillar proteins and hydrolysates, Ultrason. Sonochem. 65 (2020), 105063.
[24] J. Su, A. Cavaco-Paulo, Effect of ultrasound on protein functionality, Ultrason. Sonochem. 76 (2021) 105653, https://doi.org/10.1016/j.ultsonch.2021.105653.
[25] R. Silva, H. Ferreira, N.G. Azoia, U. Shimanovich, G. Freddi, A. Gedanken, A. Cavaco-Paulo, Insights on the Mechanism of Formation of Protein Microspheres in a Biphasic System, Mol. Pharmaceutics 9 (11) (2012) 3079–3088.
[26] J.T. He, K.Q. Bian, G.Z. Piao, Self-assembly properties of carboxylated tunicate cellulose nanocrystals prepared by ammonium persulfate oxidation and subsequent ultrasonication, Carbohydr. Polym. 249 (2020), 116835.
[27] X. Hu, D. Kaplan, P. Cebe, Determining beta-sheet crystallinity in fibrous proteins by thermal analysis and infrared spectroscopy, Macromolecules 39 (18) (2006) 6161–6170.
[28] F. Li, L. Li, G. Zhong, Y. Zhai, Z. Li, Effects of ultrasonic time, size of aggregates and temperature on the stability and viscosity of Cu-ethylene glycol (EG) nanofluids, Int. J. Heat Mass Transfer 129 (2019) 278–286.
[29] J.M. Pestman, B.F.N. Engberts, F.D. Jong, Sonochemistry: Theory and applications, Recl. Trav. Chim. Pays-Bas 113 (12) (1994) 533–542.
[30] T.S.H. Leong, G.J.O. Martin, M. Ashokkumar, Ultrasonic encapsulation – A review, Ultrason. Sonochem. 35 (2017) 605–614.
[31] L. Rayleigh, VIII., On the pressure developed in a liquid during the collapse of a spherical cavity, Philos. Mag. 34 (200) (1917) 94–98.
[32] F. Wang, H.-yang. Yu, Z.-G. Gu, L. Si, Q.-chun. Liu, X. Hu, Impact of calcium chloride concentration on structure and thermal property of Thai silk fibroin films, J. Therm. Anal. Calorim. 130 (2) (2017) 851–859.
[33] F. Wang, N. Wolf, E.-M. Rocks, T. Vuong, X. Hu, Comparative studies of regenerated water-based Mori, Thai, Eri, Muga and Tussah silk fibroin films, J. Therm. Anal. Calorim. 122 (3) (2015) 1069–1076.
[34] A. Barth, C. Zscherp, What Vibrations Tell About Proteins, Q. Rev. Biophys. 35 (4) (2002) 369–430.
[35] J. Zhang, R. Rajkhowa, J.L. Li, X.Y. Liu, X.G. Wang, Silkworm cocoon as natural material and structure for thermal insulation, Mater. Des. 49 (2013) 842–849.
[36] X. Zhang, Z.J. Pan, Microstructure Transitions and Dry-Wet Spinnability of Silk Fibroin Protein from Waste Silk Quilt, Polymers 11 (10) (2019) 1622.
[37] S. Lu, J. Li, S. Zhang, Z. Yin, T. Xing, D.L. Kaplan, The influence of the hydrophilic–lipophilic environment on the structure of silk fibroin protein, J. Mater. Chem. B 3 (13) (2015) 2599–2606.
[38] F. Zhang, J.N. Wang, B.Q. Zuo, Effect of Aqueous Ethanol Treatment on the Electrospun SF Nanofiber Mats, C. Bioinformatics and Biomedical Engineering (iCBBE) 2010 4th International Conference on 2010 1-4.
[39] H.C. Wu, F.W. Shen, X. Hong, W.V. Chang, H. Winet, Monitoring the degradation process of biopolymers by ultrasonic longitudinal wave pulse-echo technique, Biomaterials 24 (22) (2003) 3871–3876.
[40] H.Y. Zheng, B.Q. Zuo, Functional silk fibroin hydrogels: preparation, properties and applications, J. Mater. Chem. B 9 (5) (2021) 1238–1258.
[41] H.Y. Wang, Y.Y. Chen, Y.Q. Zhang, Processing and characterization of powdered silk micro- and nanofibers by ultrasonication, Mater. Sci. Eng. C 48 (2015) 444–452.
[42] Y.Y. Wang, Y.D. Cheng, Y. Liu, H.J. Zhao, M.Z. Li, The Effect of Ultrasonication on the Gelation Velocity and Structure of Silk Fibroin, Adv. Mater. Res. 175–176 (2011) 143–148.
[43] S.K. Samal, D.L. Kaplan, E. Chiellini, Ultrasound Sonication Effects on Silk Fibroin Protein, Macromol. Mater. Eng. 298 (11) (2013) 1201–1208.
[44] P.U. Kadakia, E. Jain, K.R. Hixon, C.T. Eberlin, S.A. Sell, Sonication induced silk fibroin cryogels for tissue engineering applications, Mater. Res. Express 3 (5) (2016) 055401, https://doi.org/10.1088/2053-1591/3/5/055401.
[45] T. Vu, Y. Xue, T. Vuong, M. Erbe, C. Bennet, B. Palazzo, L. Popielski, N. Rodriguez, X. Hu, Comparative Study of Ultrasonication-Induced and Naturally Self-Assembled Silk Fibroin-Wool Keratin Hydrogel Biomaterials, Int. J. Mol. Sci. 17 (9) (2016) 1497.
[46] Y. Liu, L. Yang, C. Ma, Thermal analysis and kinetic study of native silks, J. Therm. Anal. Calorim. 139 (1) (2020) 589–595.
[47] J.W. Song, C.J. Chen, S.Z. Zhu, M.W. Zhu, J.Q. Dai, U. Ray, Y.J. Li, Y.D. Kuang, Y. F. Li, N. Quispe, Y.G. Yao, A. Gong, U.H. Leiste, H.A. Bruck, J.Y. Zhu, A. Vellore, H. Li, M.L. Minus, Z. Jia, A. Martini, T. Li, L.B. Hu, Processing bulk natural wood into a high-performance structural material, Nature 554 (2018) 224–228.
[48] H. Zhu, S. Zhu, Z. Jia, S. Parvinian, Y. Li, O. Vaaland, L. Hu, T. Li, Anomalous scaling law of strength and toughness of cellulose nanopaper, Proc. Natl. Acad. Sci. 112 (29) (2015) 8971–8976.
[49] Q. Yuan, J. Yao, L. Huang, X. Chen, Z. Shao, Correlation between structural and dynamic mechanical transitions of regenerated silk fibroin, Polymer 51 (26) (2010) 6278–6283.
[50] J. Yin, E. Chen, D. Porter, Z. Shao, Enhancing the Toughness of Regenerated Silk Fibroin Film through Uniaxial Extension, Biomacromolecules 11 (11) (2010) 2890–2895.
[51] W. Liu, C.R. Carlisle, E.A. Sparks, M. Guthold, The mechanical properties of single fibrin fibers, J. Thromb. Haemostasis 8 (2010) 1030–1036.
[52] X. Wang, J.A. Kluge, G.G. Leisk, D.L. Kaplan, Sonication-induced gelation of silk fibroin for cell encapsulation, Biomaterials 29 (8) (2008) 1054–1064.
[53] W. Wang, L.J. Rather, K. Gong, Q. Zhou, T. Zhang, Q. Li, Effects of Ultrasonic Treatment on Hydrophilicity and Thermal Stability of Silk, Macromol. Mater. Eng. 304 (12) (2019) 1900364, https://doi.org/10.1002/mame.v304.1210.1002/mame.201900364.

[54] F.L. Mi, Y.M. Lin, Y.B. Wu, S.S. Shyu, Y.H. Tsai, Chitin/PLGA blend microspheres as a biodegradable drug-delivery system: phase-separation, degradation and release behavior, Biomaterials 23 (15) (2002) 3257–3267.
[55] E.T. Baran, K. Tuzlakoğlu, J.F. Mano, R.L. Reis, Enzymatic degradation behavior and cytocompatibility of silk fibroin–starch–chitosan conjugate membranes, Mater. Sci. Eng. C 32 (6) (2012) 1314–1322.
[56] F. Wang, H. Liu, Y. Li, Y. Li, Q. Ma, J. Zhang, X. Hu, Tunable Biodegradable Polylactide-Silk Fibroin Scaffolds Fabricated by a Solvent-Free Pressure-Controllable Foaming Technology, ACS Appl. Bio Mater. 3 (12) (2020) 8795–8807.
[57] F. Wang, H.Y. Yu, Q.C. Liu, Q.Y. Ma, Z.G. Gu, Structure and Kinetics of Thermal Decomposition Mechanism of Novel Silk Fibroin Films, Acta Phys.-Chim. Sin. 33 (2) (2017) 344–355.
[58] P.R. Sivashankari, M. Prabaharan, Three-dimensional porous scaffolds based on agarose/chitosan/graphene oxide composite for tissue engineering, Int. J. Biol. Macromol. 146 (2020) 222–231.
[59] F. Wang, H. Wu, V. Venkataraman, X. Hu, Silk fibroin-poly(lactic acid) biocomposites: Effect of protein-synthetic polymer interactions and miscibility on material properties and biological responses, Mater. Sci. Eng. C 104 (2019), 109890.
[60] J. Dong, Q. Sun, J.-Y. Wang, Basic study of corn protein, zein, as a biomaterial in tissue engineering, surface morphology and biocompatibility, Biomaterials 25 (19) (2004) 4691–4697.
[61] K. Zhang, H. Zheng, S. Liang, C. Gao, Aligned PLLA nanofibrous scaffolds coated with graphene oxide for promoting neural cell growth, Acta Biomater. 37 (2016) 131–142.
[62] F.J. Jiang, K. Liu, M.H. Zhao, X.C. Tao, X. Hu, S.Z. Lu, Tunable High-Molecular-Weight Silk Fibroin Polypeptide Materials: Fabrication and Self-Assembly Mechanism, ACS Appl. Bio Mater. 3 (5) (2020) 3248–3259.